Journal of Alloys and Compounds 930 (2023) 167309

Contents lists available at ScienceDirect

Journal of Alloys and Compounds

journal homepage: www.elsevier.com/locate/jalcom

Influence of isothermal omega precipitation aging on deformation mechanisms and mechanical properties of a β-type Ti-Nb alloy

S. Pilz [a,*], A. Hariharan [a], F. Günther [b,c], M. Zimmermann [b,c], A. Gebert [a]

[a] Institute for Complex Materials, Leibniz IFW Dresden, Helmholtzstr. 20, D-01069 Dresden, Germany
[b] Institute of Materials Science, TU Dresden, Helmholtzstr. 7, D-01069 Dresden, Germany
[c] Fraunhofer Institute for Material and Beam Technology (Fraunhofer IWS), Winterbergstr. 28, D-01277 Dresden, Germany

ARTICLE INFO

Article history:
Received 12 July 2022
Received in revised form 12 September 2022
Accepted 20 September 2022
Available online 23 September 2022

Keywords:
Beta titanium alloys
Omega phase
Deformation twinning
Martensitic transformation
Mechanical properties

ABSTRACT

In this study, the influence of ω_{iso} precipitates on the active deformation mechanisms and the mechanical properties of the biomedical β-type Ti-40Nb alloy are revealed. Low temperature heat treatments (aging) at 573 K for durations up to 108.0 ks were carried out for a cold-rolled and recrystallized sample state. After an aging time of 3.6 ks the ω_{iso} phase was determined by means of synchrotron XRD and the fraction and the crystallite size of ω_{iso} increased progressively with increasing aging time. Due to the high intrinsic Young's modulus of the ω_{iso} phase, the Young's modulus increased gradually with the aging time from 63 GPa, for the recrystallized reference condition, to values of 70 GPa (3.6 ks), 73 GPa (14.4 ks), 81 GPa (28.8 ks) and 96 GPa (108.0 ks). Depending on the aging time, also a change of the active deformation mechanisms occurred, resulting in significantly altered mechanical properties. For the single β-phase reference microstructure, stress-induced martensite (SIM) formation, $\{332\}\langle 11\bar{3}\rangle$ twinning and dislocation slip were observed under tensile loading, resulting in a low 0.2% proof stress of around 315 MPa but a high elongation at fracture of 26.2%. With increasing aging time, SIM formation and mechanical twinning are progressively hindered under tensile loading. SIM formation could not be detected for samples aged longer than 3.6 ks. The amount and thickness of deformation twins is clearly reduced with increasing aging time and for samples aged longer than 14.4 ks deformation twinning is completely suppressed. As a result of the changed deformation mechanisms and the increase of the critical stress for slip caused by ω_{iso}, the 0.2% proof stress of the aged samples increased gradually from 410 MPa (3.6 ks) to around 910 MPa (108.0 ks). With regard to application as new bone implant material, a balanced ratio of a low Young's modulus of E = 73 GPa and higher 0.2% proof stress of 640 MPa was achieved after an aging time of 14.4 ks.

1. Introduction

New β-type Ti-Nb alloys show great potential to become the next generation of materials for load-bearing implants, as they offer several advantages compared to the established alloys, such as stainless steel, Co-Cr and α + β Ti alloys [1,2]. For example, β-type Ti-Nb alloys exhibit remarkable low Young's modulus values in the range of only 60–65 GPa in solution-treated condition [3]. This provides an opportunity to reduce stress shielding effects which are presently caused by the large mismatch of the Young's modulus values of clinically used metallic implant materials (100–230 GPa) and of cortical bone (10–30 GPa) [4]. The strong surface passivation ability of β-type Ti-Nb alloys in bio-fluids results in an excellent corrosion resistance and very low metal release rates which in consequence, supports bone cell activity [5,6].

However, a current drawback of different kinds of β-type Ti-Nb-based alloys is their only moderate static and cyclic strength in the solution-treated state compared to Ti-6Al-4 V, the current benchmark Ti alloy for load bearing bone implants [7–9]. In order to increase the strength of this new alloy class while retaining a low Young's modulus, different thermomechanical processing strategies have been extensively studied. The influence of various hardening mechanisms, e.g., work hardening, precipitation hardening, or grain boundary strengthening have been investigated [3,8,10–16]. These processing strategies can include hot and/or cold deformation such as rolling or swaging combined with aging heat treatments to precipitate the α and/or ω phase as well as with solution or recrystallization annealing. Several studies showed that the static strength of β-type Ti-Nb-based alloys (Ti-29Nb-13Ta-4.6Zr, Ti-40Nb, Ti-45Nb) can be significantly increased (up to around 900 MPa yield

* Corresponding author.
E-mail address: s.pilz@ifw-dresden.de (S. Pilz).

https://doi.org/10.1016/j.jallcom.2022.167309

strength) by work hardening, e.g., cold rolling [3,12,16–18]. However, work hardening was found to be ineffective for increasing the fatigue strength, and is therefore, not suitable to improve the overall mechanical properties of β-type Ti-Nb-based alloys [13,15,16]. Grain boundary hardening by grain refinement is also an appropriate method to enhance the strength of β-type Ti-Nb alloys without altering their Young's modulus, but until now by this approach only moderate yield strength levels of 300–500 MPa could be reached [3,8,19].

In conclusion, the generation of α or ω precipitates in solution-treated or deformed β-type Ti alloy states appears to be the only promising approach to obtain static and fatigue strength values which reach the high level of those of Ti-6Al-4 V (yield strength ≈ 860–960 MPa, fatigue strength ≈ 550 MPa) [12,14,19–22].

However, the α and the ω phase have significantly higher intrinsic Young's moduli (E(ω) ≈ 153 GPa, E(α) ≈ 115 GPa [23]) than the β phase (E(β) ≈ 60–65 GPa[3,4]). Therefore, an increase of their fraction in the microstructure leads to an increased Young's modulus of the alloy. In order to keep this value as low as possible while increasing the strength, aging treatments must be in detail defined regarding suitable aging temperature and/or time. Although the ω phase has a higher Young's modulus than the α phase, nano-sized ω precipitates were found to be more appropriate as they can lead to strong precipitation hardening in β-type Ti-Nb-based alloys, like Ti-29Nb-13Ta-4.6Zr, even at low volume fractions [10,16]. The ω phase has a trigonal or hexagonal lattice structure, depending on the solute content of the β-type alloy, and can form during quenching from the β phase field (athermal ω) or during isothermal heat treatment at low temperatures (isothermal ω; ω_{iso}) [24].

Precipitates of ω_{iso} not only introduce precipitation hardening, but can also alter the active deformation mechanisms of β-type Ti-based alloys. For β-type Ti-based alloys various deformation mechanisms have been observed [25], including {332} and {112} twinning [26–31], stress- or deformation-induced phase transformations (e.g., β → α'', β → ω) [17,32–36], as well as dislocation slip. The activated deformation mechanisms depend mainly on the chemical composition of the β-type Ti alloy, but also on the processing history [37,38].

Various authors [39–43] showed for selected β-type Ti alloys (Ti-15Mo, Ti-20Mo, Ti-7Mo-3Cr-1Fe, Ti–12 V–2Fe–1Al, Ti-36Nb) that ω_{iso} precipitates can change the active deformation mode from {332}< 113 > twinning to dislocation slip. Furthermore, the suppression of stress induced martensite (SIM) formation by ω_{iso} was observed in several studies [8,11,37,38]. Until now, the reason for this behavior is not fully understood. Some studies conducted for Ti-12Mo and Ti-26Nb (at%) attribute the change of the deformation modes to the rejection of β-stabilizing elements from the ω_{iso} precipitates. This leads to an enrichment of β-stabilizing elements in the surrounding β matrix of the alloys resulting in an enhanced β phase stability [38,44]. On the other hand, Lai et al. [37] and Xiao et al. [41] revealed for Ti-25 Nb-0.7Ta-2Zr and Ti–12 V–2Fe–1Al that ω_{iso} precipitates are strong obstacles for {110}< 110 >$_{\beta}$ shear, which is involved in the {332}< 113 > twinning and the SIM formation. Thus, densely distributed ω_{iso} precipitates suppress a long-range martensitic transformation and deformation twinning. A similar mechanism has also been proposed for oxygen added β-type Ti alloys (like Ti-(23–26)Nb-1 O (at%), Ti-29Nb-13Ta-4.6Zr-0.7 O, Ti–(21–25) Nb–2Zr–0.7Ta-(0.1–1.8)O (at%)), where the long-range martensite formation is suppressed by nano-sized lattice modulations induced by interstitial oxygen atoms [33,45–47]. Furthermore, the presence of ω_{iso} precipitates in the microstructure of β-type Ti-based alloys, like Ti–25Nb–0.7Ta–2Zr (at%), Ti–23Nb–0.7Ta–2Zr–O (at%), Ti-9Mo-5.4Al-1.6Nb-0.3Si (at%) and Ti-(12,15)Mo, leads to a localization of the plastic flow in deformation bands which are depleted of ω_{iso} precipitates [8,37,38,48,49,50]. In these so-called dislocation channels, ω_{iso} precipitates are dissolved because of dislocation movement through these ω_{iso} precipitates.

The current study aims to analyze the suitability of ω_{iso} precipitation hardening to improve the mechanical properties of the biomedical β-type Ti-40Nb alloy. The starting point was a recrystallized sample state, which in our previous studies was obtained by hot/cold rolling and subsequent recrystallization annealing [3,8,51]. It was identified as being most suitable for further studies because in this state the Ti-40Nb alloy exhibits the best compromise between a low Young's modulus (~60 GPa) and a moderate ultimate tensile strength (~500 MPa) owing to a single β-phase, grain refined microstructure [3]. According to the equilibrium α-ß diagram and the metastable ω-ß phase diagram [52] of the Ti-Nb system and the experimental findings of Moffat und Larbalestier [53] a temperature of 573 K was selected for the ω_{iso} aging heat treatment to ensure the formation of a β + ω microstructure. The impact of the aging time on the evolving microstructures and in consequence, on the tensile test performance and on the active deformation mechanism is presented and discussed.

2. Materials and methods

2.1. Alloy processing

A binary Ti-40Nb (wt%) alloy was produced from pure elements CP2-Ti (99.7%) and Nb (99.9%) by a two-step casting process. First, ingots were prepared by arc-melting under Ar atmosphere and re-melted three times to ensure a high chemical homogeneity. In the second step, a cold crucible device was used to re-melt the ingots by induction heating and cast them to a rod with a diameter of 12 mm and a length of around 100 mm. The rod was enclosed in a fused silica tube under Ar atmosphere and then subjected to solution treatment at 1273 K for 86.4 ks, followed by quenching into water, aiming to obtain a single ß-type sample state. The chemical composition of the samples was determined as 59.6Ti-40.4Nb by inductively coupled plasma optical emission spectrometry (ICP-OES). Further details of the sample preparation and characterization have been described previously [3,51,54].

Cold rolling was performed with a thickness reduction of 20% per rolling pass. After a total thickness reduction of 74%, recrystallization annealing was carried out at 1073 K for 1.2 ks under Ar atmosphere followed by water quenching. Cold rolling was continued until a total thickness reduction of 93% was reached. The final sheet (thickness = 0.8 mm) was recrystallized at 1073 K for 1.2 ks and quenched into water. This sample state will be denoted as "RC" (recrystallized) hereafter.

Subsequently, ω_{iso} aging heat treatments were carried out at 573 K for holding times of 3.6 ks, 14.4 ks, 28.8 ks and 108.0 ks. Therefore, samples with a length of around 50 mm were cut from the recrystallized sheet. To minimize the uptake of interstitial elements such as oxygen and nitrogen, samples were sealed in fused silica tubes under Ar atmosphere. After the ω_{iso} aging heat treatments, rapid cooling was conducted by water quenching. The oxygen and nitrogen content of the samples was analyzed by carrier gas hot extraction (LECO TC-436DR). For the recrystallized sample (RC), an O content of 0.0752 wt% and a N content of 0.018 wt% was determined. Similar values were measured after the different aging treatments with a maximum deviation of 0.006 wt% for O and 0.003 wt% for N.

The aged samples will be denoted by their aging time as A3.6 (t = 3.6 ks), A14.4 (t = 14.4 ks), A28.8 (t = 28.8 ks) and A108.0 (t = 108.0 ks), respectively.

2.2. Microstructural and mechanical characterization

Specimens for microstructural investigations were mechanically ground using SiC emery paper (P400 – P2500). For the final polishing

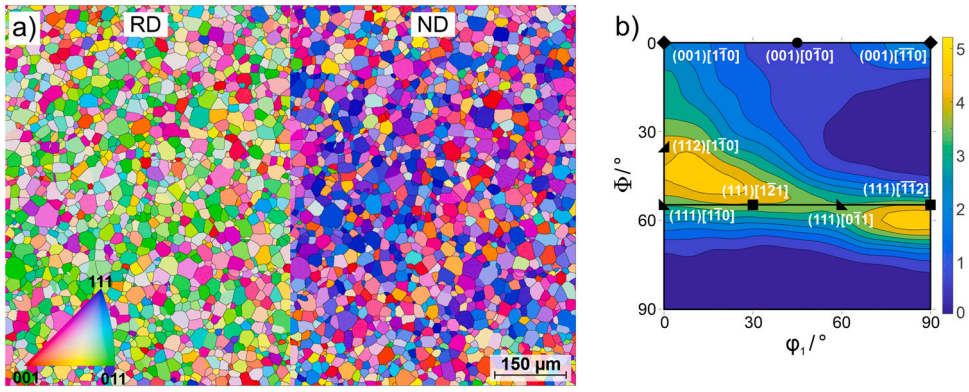

Fig. 1. Microstructure of RC state obtained from EBSD measurements. (a) Crystallographic orientation maps taken perpendicular to the RD and the ND. (b) Texture in terms of ODF phi_2 = 45° section.

step, a solution of colloidal SiO_2 (90 vol%) and H_2O_2 (10 vol%) was used. Scanning electron microscope (SEM) imaging and electron backscatter diffraction (EBSD) analysis was carried out with a Zeiss Leo Gemini 1530 equipped with an EBSD system (Bruker e-Flash^{HR}). Analyses were performed on longitudinal cross sections of the samples in the initial state and after tensile tests. For the evaluation of EBSD measurements and the texture analysis, the open-source toolbox MTEX (v.5.0.1) [55] was used. Site-specific transmission electron microscopy (TEM) lamellae around 80 nm thick were prepared from A108.0 ample states using the focused ion beam (FIB) Helios 5 CX on a Cu grid. The lamellae were subjected to low-kV cleaning to remove any Ga contamination. Transmission electron microscopy was carried out in a Philips Tecnai F20 (TEM, 200 kV) using a double-tilt holder. Post-processing of the diffraction data was performed using the SingleCrystal software (version 4.0).

Uniaxial tensile tests were carried out using an Instron 5869 device with a cross head velocity of 0.045 mm/min. Flat bar tension specimens with 0.8 mm thickness, 2 mm width and with a gauge length of 8 mm were cut by means of electro-discharge machining. The tensile axis of the specimens was parallel to the rolling direction (RD) of the sheet. The strain was recorded with a laser extensometer (Fiedler Optoelektronik). For each sample state at least three samples were tested. Selected tensile test samples were analyzed by SEM and EBSD after fracture.

Synchrotron X-ray diffraction experiments (SXRD) were performed at the High Energy Materials Science (HEMS) beamline [56] at PETRA III (Deutsches Elektronen-Synchrotron, DESY) for undeformed sample states and for tensile tested samples in the area of the fracture tip. The experiments were conducted using an X-ray beam with an energy of 103.978 keV, collimated to a size of 500 × 500 µm^2. Diffraction Patterns were collected with a flat panel detector (XRD 1622, PerkinElmer) at a sample to detector distance of 1683 mm. A LaB_6 powder specimen was measured for calibration purpose. Quantitative phase analysis of the diffraction patterns was performed with the Rietveld method using the software MAUD (version 2.993) [57]. The structure model for the β phase was described by a cubic space group *Im*-3*m* [58], for the ω phase with a hexagonal space group *P*6/*mmm* [59] and the α" phase was described by the orthorhombic space group *Cmcm* [60].

3. Results

3.1. Microstructure of the recrystallized and aged sample states

In the course of this study, the cold-rolled and recrystallized state (RC) was considered as reference state in the analysis of the effect of further ω_{iso} aging heat treatment (A states) at 573 K for different durations.

Results regarding the microstructure and texture of Ti-40Nb in the RC state are shown in Fig. 1. The EBSD measurements perpendicular to the rolling direction (RD) as well as to the normal direction (ND) reveal a complete recrystallized microstructure with equiaxed grains. The mean equivalent diameter of the grains is determined as d = 24.6 µm ± 0.6 µm. The inverse pole figure color coding of the EBSD maps already shows the existence of a crystallographic texture after the recrystallization annealing. For a detailed description of the texture, the orientation density function (ODF) is calculated based on three measurements and the phi_2 = 45° section of the ODF is given in Fig. 1(b). A clear γ-fiber ({111} || ND) and α-fiber (< 111 > || RD) are observed. Both fiber textures are typical recrystallization textures of β-type Ti alloys after flat rolling and subsequent recrystallization annealing [61,62]. For the ω_{iso} aged (A) sample states no changes concerning the average grain size or texture were observed even after the longest aging time of 108.0 ks.

To study the phase composition of the RC sample and of the samples after the additional ω_{iso} aging heat treatments, SXRD measurements were carried out and are shown in Fig. 2. For the RC state only reflexes corresponding to the β phase can be identified. After an aging time of 3.6 ks (sample state A3.6) an additional reflex at around 5.65° appears, which can be assigned to diffraction at the [11-22]- and [3031]-planes of the ω_{iso} phase. With increasing aging time, the intensity of this reflex increases and additional reflexes belonging to the ω_{iso} phase become apparent (marked by red dots in Fig. 2). For the investigated aging times of up to 108 ks (sample A108.0), no reflexes belonging to additional phases like the α phase are detected. This is in accordance with early observations of Moffat and Larbalestier [53].

Quantitative phase analysis of the diffraction patterns was carried out using the Rietveld method and phase fraction and mean crystallite size of the ω phase are summarized in Table 1. With increasing aging time, the ω phase fraction increases from around 10 wt% (A3.6) to around 30 wt% (A108.0). This increase is accompanied by a growth of the ω crystallites from around 5 nm (A3.6) to around 13 nm (A108.0).

The single β-type microstructure of the RC state was also confirmed by TEM analysis. A typical bright-field TEM image and the corresponding selected area electron diffraction pattern (SAED) of the RC state are shown in Fig. 3(a). The SAED patterns can be indexed as a bcc β-phase and no secondary phase could be detected. The results of the SXRD and SAED analyses did not reveal the presence of any secondary phases such as ω phase or α″ martensite before the aging treatment. A dark field TEM image of the Ti-40Nb sample aged for 108.0 ks is shown in Fig. 3(b) together with the corresponding SAED as inset. It is seen that ω_{iso} precipitates (bright phase) are densely and homogeneously distributed in the β phase matrix. After an aging time of 108.0 ks, the precipitates have dimensions of

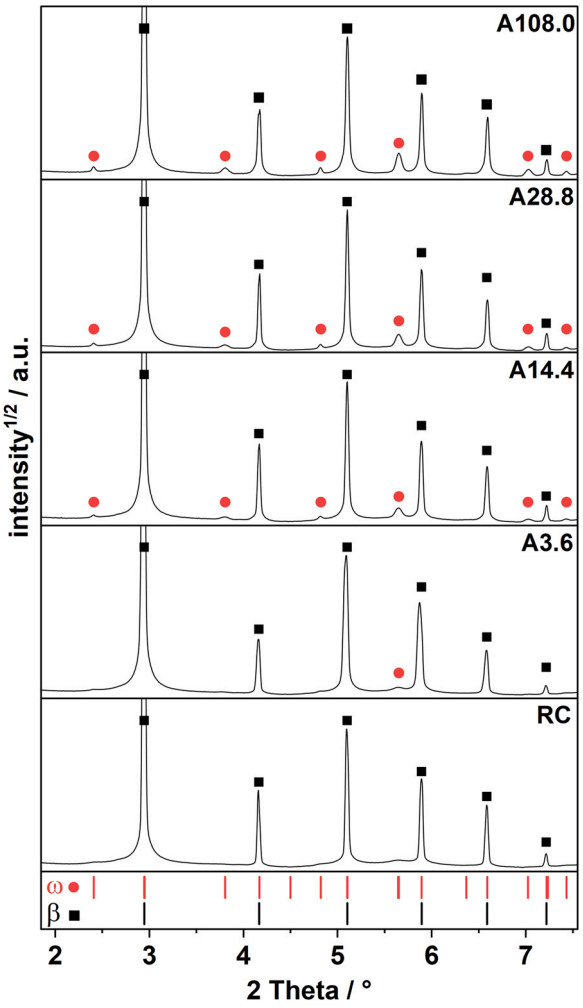

Fig. 2. SXRD patterns of Ti-40Nb alloy after recrystallization annealing (RC) and after subsequent aging at 573 K for 3.6 ks (A3.6), 14.4 ks (A14.4), 28.8 ks (A28.8) and 108.0 ks (A108.0).

Table 1
Phase percentage and mean crystallite size of the ω phase determined from SXRD by the Rietveld method.

	ω phase percentage in wt%	mean ω crystallite size in nm
A3.6	9.9 ± 0.7	5.0 ± 0.5
A14.4	22.1 ± 0.8	8.6 ± 0.3
A28.8	24.4 ± 0.6	11.0 ± 0.5
A108.0	30.3 ± 0.7	12.6 ± 0.5

around 15 nm and below. This emphasizes the sluggish ω_{iso} precipitation process that is caused by the fact that the solute diffusion of Nb in Ti, decreases exponentially with the Nb content in β-type Ti-Nb alloys [52,53]. In the SAED pattern, typical diffraction spots are visible at the 1/3 and 2/3 $\{112\}_\beta$ reflection positions of the β matrix, indicating the hexagonal crystal structure of the ω_{iso} phase and the orientation relationships of $[011]_\beta \| [\bar{1}2\bar{1}0]_\omega$ and $(11\bar{1})_\beta \| (0001)_\omega$ [8,43].

3.2. Mechanical properties

Selected engineering tensile stress-strain curves of Ti-40Nb samples in the RC state and after different aging times at 573 K (A states) are depicted in Fig. 4. Here, a magnified view of the linear region is given in Fig. 4(a) together with a visualization of the extrapolated linear elastic regions of the different sample states (red dashed lines).

The stress-strain curve of RC shows a characteristic double yielding behavior that is provoked by the stress induced transformation of the metastable β phase into the martensitic α" phase [3,37,51,63]. In the curve progression, the first yield point can be associated with the beginning of the SIM formation, which leads to a deviation from the linear elastic behavior once the critical stress for the martensite formation is reached [64]. The second yield point correlates with the beginning of the plastic deformation of the β phase and the previously formed α" phase [65]. The precipitation of the ω_{iso} phase during the aging treatment has a clear influence on the curve progression and on the mechanical behavior of the Ti-40Nb alloy. With increasing aging time (A3.6 to A108.0), the pronounced double yielding behavior observed for the RC state devolves progressively into a complete linear elastic behavior for A108.0. Furthermore, a clear transition from a continuous to a discontinuous yielding behavior takes place with increasing aging time.

The mean values of the mechanical properties of the different aging states, derived from at least three tensile tests per state, are summarized in Fig. 5 together with the standard deviation.

In the RC condition, with a single ß phase microstructure, Ti-40Nb shows a 0.2% proof stress of about 315 MPa and an ultimate tensile strength (UTS) of around 500 MPa. The low 0.2% proof stress can be attributed to the low stress level that is needed for the initiation of the SIM formation [19]. The formed ω_{iso} precipitates lead to a gradual increase of the 0.2% proof stress and the UTS with increasing aging time. The UTS shows a nearly logarithmic dependence on the aging time. For the sample state A3.6, the 0.2% proof stress and UTS is increased by around 100 MPa to 410 MPa and 615MPa compared to RC. In contrast, for state A108.0 a significantly increased 0.2% proof stress and UTS of around 900 MPa is reached. This corresponds to an increase of the 0.2% proof stress by a factor of 2.5 when compared to the initial RC condition.

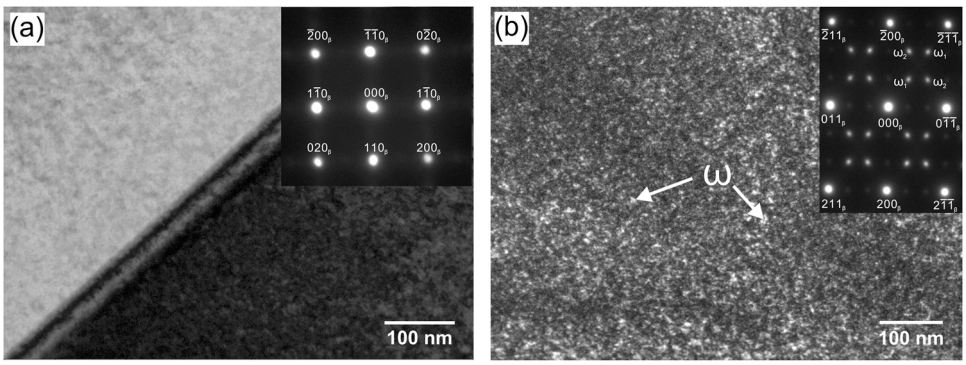

Fig. 3. (a) Bright field TEM image of the Ti-40Nb alloy in the recrystallized (RC) state, and the corresponding selected area diffraction pattern (inset). The beam is parallel to $[001]_\beta$. (b) Dark field TEM image of Ti-40Nb alloy aged at 573 K for 108.0 ks (A108.0), and the corresponding selected area diffraction pattern (inset). The beam is parallel to $[01\text{-}1]_\beta$.

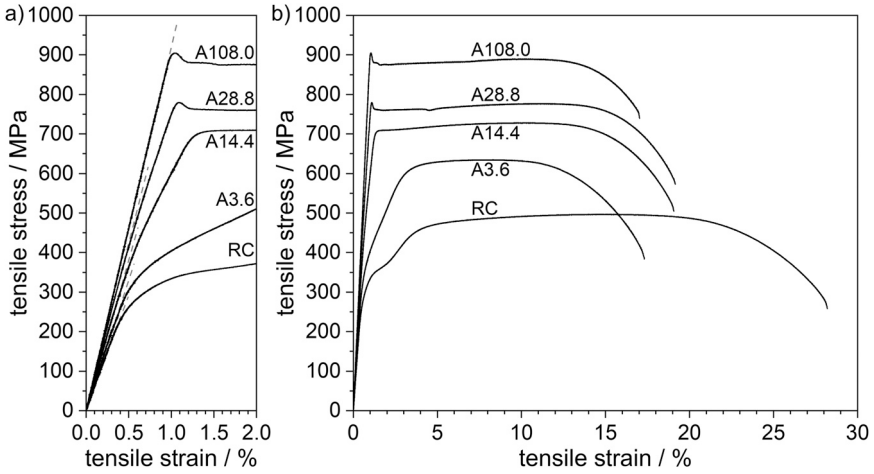

Fig. 4. Engineering stress-strain curves of Ti-40Nb alloy after recrystallization annealing (RC) and after subsequent aging at 573 K for 3.6 ks (A3.6), 14.4 ks (A14.4), 28.8 ks (A28.8) and 108.0 ks (A108.0). a) Magnified view of the linear region. Red dashed lines correspond to the extrapolated linear elastic regions of the different sample states. b) Complete stress-strain curves.

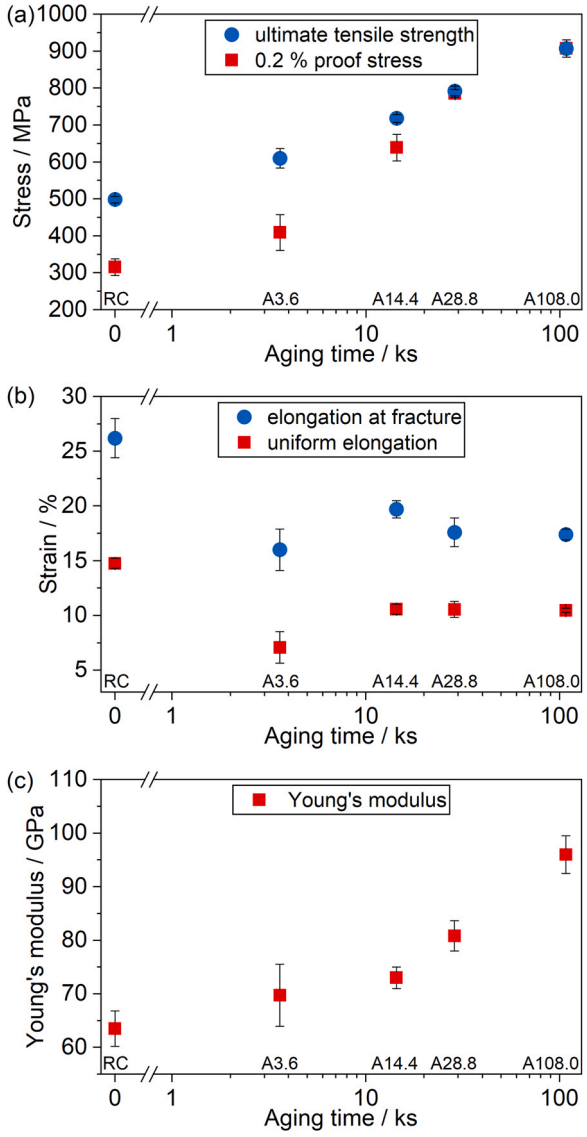

Fig. 5. Mechanical properties of Ti-40Nb alloy after recrystallization annealing (RC; aging time = 0ks) and after subsequent aging at 573 K for 3.6 ks (A3.6), 14.4 ks (A14.4), 28.8 ks (A28.8) and 108.0 ks (A108.0).

The strain values presented in Fig. 5(b) demonstrate that the uniform elongation (u_e) derived by the Considére criterion [66] as well as the total elongation at fracture (e_t) are reduced by ω_{iso} precipitates. In the RC state, Ti-40Nb reaches a uniform elongation of 14.5% and an elongation at fracture of 26.8%. For the aged sample conditions, sample A14.4 shows the highest e_t (10.6%) and u_e (19.7%) values. A lower aging time (A3.6) results in a significant reduction of both values to 7.1% and 16.0%, respectively. For aging times longer than 14.4 ks, e_t and u_e decrease again to reach values of 10.3% and 17.4%, respectively, at an aging time of 108.0 ks (A108.0).

The influence of the ω_{iso} precipitation annealing time on the Young's modulus is shown in Fig. 5(c). For the RC condition, a Young's modulus of 63 GPa was determined. Even a short aging time of 3.6 ks results in a slightly increased Youngs's modulus of around 70 GPa (A3.6). Due to the growing phase fraction and crystallite size of ω_{iso}, the Young's modulus values of the alloy states increase further with increasing aging time to values of 73 GPa (A14.4), 81 GPa (A28.8) and 96 GPa (A108.0).

3.3. Deformation microstructures

To investigate the active deformation mechanisms and the resulting microstructural changes, EBSD and SXRD analyses were performed on the samples after tensile testing. The SXRD measurements were conducted at the fracture tip of the samples and the results are depicted in Fig. 6. Clear reflections corresponding to the martensitic α'' phase are identified for the RC and the A3.6 state after the tensile test. For the latter one the α'' phase fraction was significantly reduced to 21 wt% when compared to the RC state (99 wt %). SXRD patterns of the samples A14.4, A28.8 and 108.0 show only reflections belonging to the β and the ω phase and no reflexes corresponding to the martensitic α'' phase were observed.

The microstructure of the samples after tensile tests is presented by EBSD measurements depicted in Fig. 7. To avoid mis-indexing caused by the pseudo-cubic symmetry of the orthorhombic α''-martensite, the α'' phase was also indexed as bcc β phase [37,67,68]. In the RC state, deformation twins of the β phase and α''-lamellae are present in the microstructure of the alloy. The deformation twins are identified as {332}< 113 > -twins and are characterized by a misorientation of ~50.5° around the < 110 > -direction. Although the α'' phase is not considered for indexing, α''-lamellae can be identified by a misorientation angle of a few degrees to the surrounding matrix when indexed as β phase [37,67]. Furthermore, clear orientation gradients are visible within the deformed β grains and the

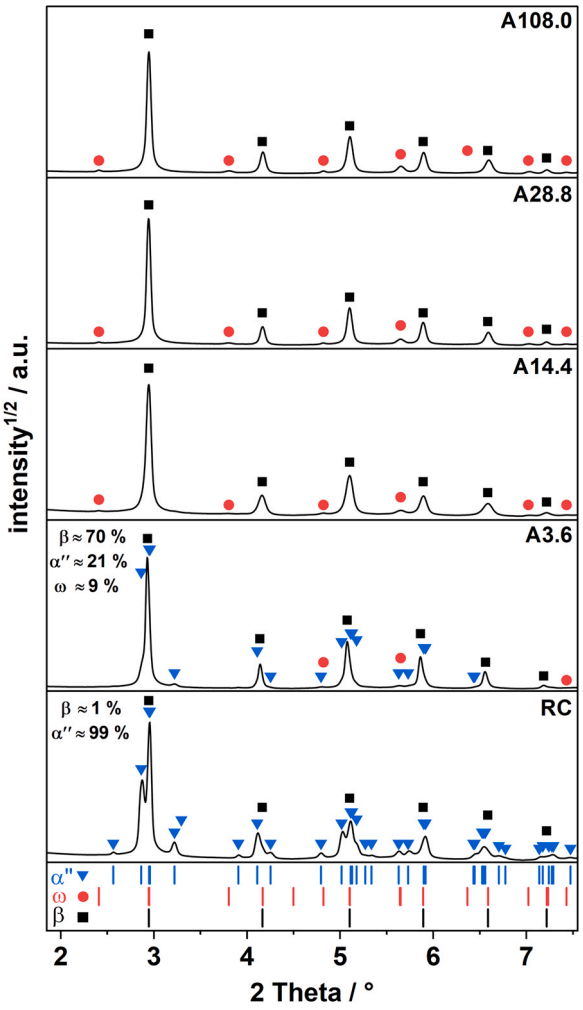

Fig. 6. SXRD patterns of the tensile tested specimen of Ti-40Nb alloy after recrystallization annealing (RC) and after subsequent aging at 573 K for 3.6 ks (A3.6), 14.4 ks (A14.4), 28.8 ks (A28.8) and 108.0 ks (A108.0).

deformation twins that can be traced back to dislocation slip and the resulting lattice rotation. The precipitation of the ω_{iso} phase leads to a clear reduction of the amount and width of deformation twins with increasing aging time. For aging times longer than 14.4 ks (A28.8 & A108.0), no deformation twins were apparent along the whole cross-section area of the tensile samples. Also, no α'' lamellae can be identified for aging times longer than 3.6 ks. Simultaneously, ω_{iso} precipitates lead to localization of the plastic deformation during tensile testing. This becomes apparent from mostly parallel slip lines especially near grain boundaries and the slip of relatively large grain areas (see insets of Fig. 6(b) & (d)).

4. Discussion

The results of this study demonstrate that the mechanical properties of Ti-40Nb can be greatly influenced by ω_{iso} precipitates generated by aging heat treatments. It is found that ω_{iso} precipitates change the active deformation mechanisms of the Ti-40Nb alloy during tensile deformation. These findings will be discussed in detail in the following sections.

4.1. Altering the active deformation mechanism by ω_{iso} aging

In β-type Ti alloys the active deformation mechanisms depend to a large extend on the β phase stability. While plastic deformation in stable β-type Ti alloys typically proceeds by dislocation slip, additional deformation mechanisms like deformation twinning and SIM formation are observed for alloys with a low β phase stability. Based on the bond order (B_o) - d-orbital energy level (M_d) phase stability model (B_o = 2.869, M_d =2.441 eV), and on the e/a ratio (e/a = 4.256), a low β phase stability can be concluded for Ti-40Nb [3,69].

The results of the microstructural observations after tensile tests (Fig. 6 & Fig. 7) reveal that the plastic deformation of Ti-40Nb in the RC state is carried by dislocation slip, {332}< 113 > deformation twinning and stress-induced formation of α''-martensite. This is in accordance with active deformation modes reviewed in literature for this alloy in the recrystallized or solution treated condition [3,8,11,33,70]. Depending on the aging time and therefore on the volume fraction and size of ω_{iso} precipitates, a change of the active deformation mechanisms is observed in the current study. For an aging time of 3.6 ks (A3.6), the EBSD and SXRD measurements (Fig. 6 & Fig. 7), SEM images (Supplementary 1) and the still pronounced double yielding in the stress-strain curve (Fig. 4) verify that SIM formation is not completely suppressed by the formed ω_{iso} precipitates. But the fraction of α''-phase present in the deformed microstructure is significantly reduced from around 99 wt% to around 21 wt% [3]. These results imply that depending on the size and phase fraction of the ω_{iso} precipitates the formation of SIM is strongly inhibited. The clear increase of the 0.2% proof stress (by about 30%) that can be considered as the critical stress for SIM (σ_{SIM}) formation, confirms this behavior. Kim et al. [44,71] and Tahara et al. [63] also determined a significant rise of σ_{SIM} for binary β Ti-Nb alloys after applying similar aging treatments (T = 573 K, t = 3.6 ks). Furthermore, an increase of the critical stress for slip was observed in these studies, which is in accordance with the present ones. Two reasons for the influence of ω_{iso} precipitates on the SIM formation can be considered according to literature. The formation of ω_{iso} is thermally activated by a diffusive growth mechanism, whereby Nb atoms are rejected out of the ω_{iso} phase [72]. As a result, the concentration of Nb in the surrounded β matrix is increased. With increasing Nb concentration, the β phase stability increases and the martensite start temperature is lowered, thereby σ_{SIM} is increased [71]. Lai et al. [37] demonstrated by atom probe tomography for Ti-25Nb-0.7Ta-2Zr (at%) that the suppression of SIM formation by ω_{iso} cannot be explained only by the enrichment of β stabilizers in the β matrix. Rather, formation of SIM is also hindered by the ω_{iso} precipitates themselves. The decisive factors for this are the homogeneous and dense distribution of ω_{iso} precipitates in the β matrix and the much higher shear modulus on the $\{11\bar{2}0\}_\omega$ planes when compared to C'_β (shear modulus along $\{1\bar{1}0\}_\beta\langle 1\bar{1}0\rangle_\beta$) [38]. These conditions suppress the long-range formation of SIM by impeding the necessary shuffle of $\{1\bar{1}0\}_\beta$ planes along $\langle 1\bar{1}0\rangle_\beta$ directions. This competition and subsequent superposition between the two mechanisms makes it challenging to resolve the most dominant factor that influences the deformation behavior. However, it can be stated that both mechanisms are enhanced with increasing aging time, which corresponds with the increase of the size and phase fraction of ω_{iso} precipitates that was detected by Rietveld refinement (Table 1).

Thus, for an increased aging time of 14.4 ks (A14.4) the ω fraction increased to around 22 wt% and SIM cannot be detected in the deformed microstructure of Ti-40Nb by EBSD, SXRD and SEM imaging (Fig. 6, Fig. 7 & Supplementary 1). For the stress-strain curves, still a slight deviation from the linear elastic behavior is visible (Fig. 4(a)). An early onset of the plastic deformation can be excluded, as loading-unloading experiments until a tensile strain of 1% (σ_{max} ≈ 650 MPa) have clarified, that a complete reversibility of the deformation is observed (Supplemental 2). Such an abnormal pseudo-elastic behavior is described for cases where high amounts of oxygen are intentionally added to β-type Ti alloys [33,45,73,74]. In this case, a long-range martensite formation is suppressed by nano-sized lattice modulations of the β phase, that are induced by the interstitial

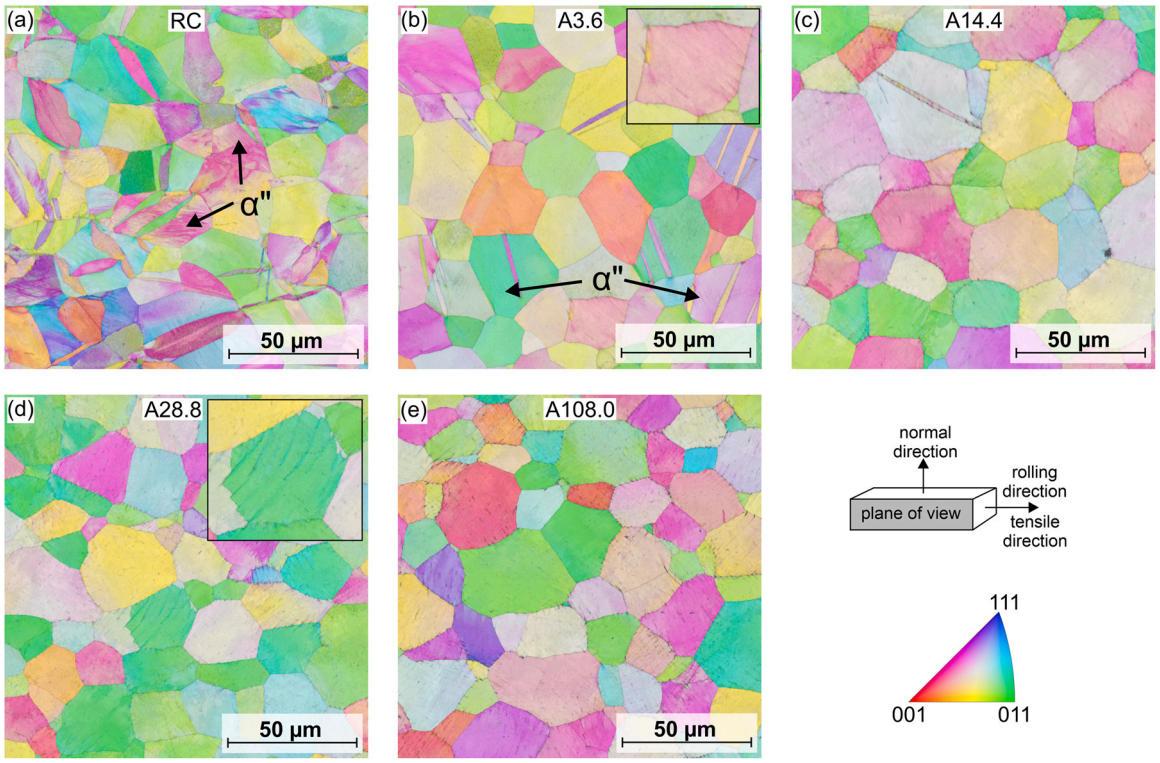

Fig. 7. Microstructure of Ti-40Nb after tensile tests obtained from EBSD measurements. Crystallographic orientation maps superimposed with the band contrast: (a) Recrystallized condition (RC) and conditions aged at 573 K for (b) 3.6 ks, (c) 14.4 ks, (d) 28.8 ks and (e) 108.0 ks. The image width of the insets in (b) and (d) is 25 µm.

oxygen atoms. The non-linear elastic behavior that is observed in the current study for ω_{iso} aged Ti-40Nb states might therefore be a result of the ω_{iso} precipitates acting as obstacles for a long-range martensite formation. With increasing aging time and thus increasing volume fraction of ω_{iso}, the deviation from the linear elastic behavior becomes smaller and for t = 108.0 ks (A108.0) a complete linear elastic behavior occurs for Ti-40Nb (Fig. 4).

The ω_{iso} annealing has also an effect on the activation of {332}< 113 > deformation twinning [27,37,39,74,75]. As obvious from Fig. 7, the amount and thickness of twins is clearly reduced with increasing size and phase fraction of the ω_{iso} precipitates and for the samples A28.8 and A108.0 deformation twinning is completely suppressed. As with SIM formation, the influences of ω_{iso} precipitates acting as barriers and of the enrichment of the β matrix with the β stabilizer Nb are hard to distinguish. Studies on the deformation behavior of binary Ti-Nb alloys showed that alloys with Nb contents higher than 41–42 wt% deform exclusively by slip at room temperature [27,39,74]. Hence, a small Nb enrichment of the β matrix of 1–2 m.% can already suppress deformation twinning in Ti-40Nb. However, for the 3.6 ks aged specimens (A3.6), some of the observed deformation twins do not propagate through the entire grain, but are stopped within the grain, as shown in Fig. 7(b). This indicates a barrier effect of ω_{iso} precipitates on the twin propagation in Ti-40Nb that was also observed by Sun et al. for a ω_{iso} aged Ti-12Mo alloy [75].

In β-type Ti alloys deformation twinning and SIM formation can be accompanied by the stress-induced formation of the ω phase [34,35]. For the RC sample, which showed the highest amount of deformation twinning and SIM formation, the stress-induced ω phase could not be detected in the deformed microstructure by means of SXRD.

The deformation behavior of Ti-40Nb by dislocation slip is also altered by the formed ω_{iso} precipitates. Several authors have described a localization of the plastic flow in β-type Ti alloys when ω_{iso} precipitates are present in the microstructure [37,38,48,49,50]. Thereby, dislocation slip is limited to a series of ω-devoid channels that are formed by cutting the ω precipitates through dislocations leading to a back transformation of the ω phase to the β phase [37,48]. Due to the depletion of ω precipitates, these channels become easy paths for the further dislocation movement and a localization of the plastic flow in these channels occurs [8,37]. First indications for a localization of the plastic flow in Ti-40Nb can already be distinguished in some grains after an aging time of 3.6 ks (A3.6; inset Fig. 7(b)), which corresponds to a ω_{iso} fraction of around 10 wt%. As a result of the localized dislocation movement, step like structures are visible at the grain boundaries. For aging times of 14.4 ks (A14.4) and longer (A28.8 & 108.0), these steps are evident at most grain boundaries after the tensile tests (Fig. 7, Supplementary 1).

4.2. The effect of ω_{iso} aging on the mechanical properties

The active deformation mechanisms of β-type Ti alloys have a great influence on their mechanical properties. Therefore, by altering these mechanisms through ω_{iso} precipitation, the mechanical properties of Ti-40Nb are greatly changed.

The initial RC state of Ti-40Nb has a relatively low 0.2% proof stress of 315 MPa and a moderate UTS of around 500 MPa. This is in good accordance with the values reported for single β-phase Ti-(40–45)Nb alloys (0.2%YS: 315–475 MPa; UTS: 480–500 MPa) [3,11]. The reason for the low 0.2% proof stress is the already described formation of SIM during mechanical loading. Recent investigations on this specific alloy state have proven that the critical stress for SIM formation and martensite stabilization is substantially lower under fatigue loading conditions (R = −1) [8,11]. This behavior can lead to a residual deformation of the material even for stresses which are significantly below the 0.2% proof stress. For a possible application of the β-type Ti-40Nb alloy as load-bearing implant material, SIM formation must be avoided.

On the other hand, SIM formation of α'' contributes to the uniform elongation (e_u) and increases the plasticity due to the transformation induced plasticity (TRIP) effect. The strain induced by the β → α'' transformation in Ti-40Nb can be calculated from the lattice parameters of the α'' and the β phase [33,44]. Based on the lattice parameters determined by Bönisch et al. [76], the maximum transformation strain of 2.5% occurs along the $< 110 >_\beta$-direction for Ti-40Nb. For a non-textured polycrystalline Ti-40Nb sample it can therefore be assumed that the overall contribution of SIM to the total strain is significantly lower. Besides the SIM α'' formation, also deformation twinning contributes to the uniform elongation and to e_t. Zhou et al. [77] calculated the contribution of primary {332}< 113 > -twinning of different crystal orientations to the macroscopic plastic deformation. For β Ti crystals, depending on their orientation, maximum strains between 9.0% ($[001]_ß$ orientation) and 19.2% ($[122]_ß$ orientation) can be realized. For a polycrystalline β Ti sample, Lai et al. [37] estimated a maximum deformation strain of 12.84%. Therefore, it can be concluded that the contribution of deformation twinning to the plastic deformation is higher than that of the SIM formation in Ti-40Nb.

Both deformation mechanisms are significantly suppressed after the aging treatment at 573 K for 3.6 ks (A3.6) due to the ω_{iso} formation (around 10 wt%). Furthermore, localization of the plastic flow in terms of dislocation channels occurs in some grains and limited stress concentration, especially at the grain boundaries occurs. As a result, e_t and u_e are considerably reduced for the aged sample A3.6, as shown in Fig. 5. Interestingly, e_t and u_e increase again for a holding time of 14.4 ks (A14.4) until u_e stays nearly constant (A28.8) and e_t decreases again with increasing holding time (A108.0). This behavior has not yet been observed for ω_{iso} aged β-type Ti alloys, but for ß-type Ti alloys to which oxygen was intentionally added [46]. The low u_e of the sample A3.6 can thus be explained by the inhomogeneous development of dislocation channels in the microstructure, leading to a local stress concentration at the grain boundaries and early crack initiation in these regions. For longer aging times, the density of dislocation channels is increased, and the deformation localization is more homogenously distributed over the sample. Since different slip systems are activated for one grain, dislocation channels intersect with each other. The interaction of the dislocations with multiple slip systems results in an increased work-hardening rate, so that necking of the sample occurs later and u_e increases. This behavior is observed for samples aged for 14.4 ks to 108.0 ks (A14.4, A28.8, A108.0).

From the summary of the mechanical properties (Fig. 5) it is obvious that precipitates of the ω_{iso} phase are effective to increase the critical stress for dislocation slip. For an aging time of 108.0 ks (A108.0), a 0.2% proof stress of around 900 MPa was achieved. This is twice as high as the value of the RC state and it is comparable with the strength values of the benchmark alloy Ti-6Al-4 V (830–950 MPa) [4]. Due to the significant fraction of ω_{iso} phase present after the long aging time, the Young's modulus is also significantly increased to about 95 GPa. This is still about 10% less than that of Ti-6Al-4 V (E = 115 GPa). With regard to the defined goal for implant applications, i.e. a balanced ratio of low Young's modulus and higher 0.2% proof stress, a final low temperature aging time at 573 K of 14.4 ks corresponding to sample state A14.4 appears to be most promising. Thereby, in comparison to the starting recrystallized RC state only a small increase of the Young's modulus of 10 GPa to E = 73 GPa occurred, but the 0.2% proof stress could be more than doubled from 315 MPa (RC) to 640 MPa (A14.4). This processing state is also superior compared to our previous finding regarding the thermomechanical processing of the Ti-40Nb alloy [3]. In this study we were able to reach similar UTS values (650–675 MPa) by a combination of cold-rolling (36%) and additional α-phase aging, but with a significant lower elongation at fracture (~7%).

5. Conclusion

In this study, the influence of ω_{iso} precipitates, obtained by aging heat treatments at 573 K for durations up to 108.0 ks on the active deformation mechanisms and the mechanical properties of the β-type Ti-40Nb alloy were revealed. For an initial recrystallized sample state, comprising a single β phase microstructure, stress-induced martensite (SIM) formation, $\{332\}\langle 11\bar{3}\rangle$ twinning and dislocation slip were observed under tensile loading. As a result of SIM and deformation twinning, only a low 0.2% proof stress of 315 MPa but a high elongation of 26.2% could be achieved for this condition. The precipitation of the ω_{iso} phase resulted in an increased suppression of SIM and deformation twinning with increasing aging time. For aging times longer than 3.6 ks SIM could not be detected in the deformed microstructure by XRD and EBSD. Deformation twinning was completely suppressed for aging times longer than 28.8 ks. Furthermore, the 0.2% proof stress of the alloy was significantly increased to around 900 MPa by ω_{iso} precipitates when the alloy was aged for 108.0 ks. Due to the high intrinsic Young's modulus of the ω phase, also the Young's modulus of the alloy was significantly increased up to 95 GPa after such long aging times.

With regard to application as new bone implant material, a balanced ratio of a low Young's modulus of E = 73 GPa and higher 0.2% proof stress of 640 MPa was achieved after an aging time of 14.4 ks.

CRediT authorship contribution statement

Stefan Pilz: Conceptualization, Methodology, Investigation, Formal analysis, Visualization, Writing – original draft, Writing – review & editing. **Avinash Hariharan:** Investigation, Writing – original draft, Writing – review & editing. **Fabian Günther:** Writing – review & editing. **Martina Zimmermann:** Writing – review & editing, Funding acquisition, Project administration, Resources, Supervision. **Annett Gebert:** Writing – review & editing, Funding acquisition, Project administration, Resources, Supervision.

Data availability

Data will be made available on request.

Declaration of Competing Interest

The authors declare that they have no known competing financial interests or personal relationships that could have appeared to influence the work reported in this paper.

Acknowledgment

The authors are grateful to Sven Donath and Dirk Seifert for technical assistance, Heike Bußkamp and Andrea Voss for chemical analyses and Dina Bieberstein and Thomas Wiek for the TEM lamellae preparation. We thank Jens Freudenberger, David Geissler and André Reck for fruitful scientific discussions. We acknowledge DESY (Hamburg, Germany), a member of the Helmholtz Association HGF, for the provision of experimental facilities. Parts of this research were carried out at PETRA III and we would like to thank Emad Maawad for assistance in using beam line P07. Beamtime was allocated for proposal I-20220421.

Funding

Funding by the Deutsche Forschungsgemeinschaft (DFG) under project GE/1106/12-1 and ZI/1006/16-1 (no 419952351) is acknowledged.

Appendix A. Supporting information

Supplementary data associated with this article can be found in the online version at doi:10.1016/j.jallcom.2022.167309.

References

[1] M. Kaur, K. Singh, Review on titanium and titanium based alloys as biomaterials for orthopaedic applications, Mater. Sci. Eng. C 102 (2019) 844–862, https://doi.org/10.1016/j.msec.2019.04.064

[2] F. Anene, C. Aiza Jaafar, I. Zainol, M. Azmah Hanim, M. Suraya, Biomedical materials: a review of titanium based alloys, Proc. Inst. Mech. Eng. Part C J. Mech. Eng. Sci. 235 (2021) 3792–3805, https://doi.org/10.1177/0954406220967694

[3] A. Helth, S. Pilz, T. Kirsten, L. Giebeler, J. Freudenberger, M. Calin, J. Eckert, A. Gebert, Effect of thermomechanical processing on the mechanical biofunctionality of a low modulus Ti-40Nb alloy, J. Mech. Behav. Biomed. Mater. 65 (2017), https://doi.org/10.1016/j.jmbbm.2016.08.017

[4] M. Geetha, A.K. Singh, R. Asokamani, A.K. Gogia, Ti based biomaterials, the ultimate choice for orthopaedic implants - A review, Prog. Mater. Sci. 54 (2009) 397–425, https://doi.org/10.1016/j.pmatsci.2008.06.004

[5] A. Gebert, D. Eigel, P.F. Gostin, V. Hoffmann, M. Uhlemann, A. Helth, S. Pilz, R. Schmidt, M. Calin, M. Göttlicher, M. Rohnke, J. Janek, Oxidation treatments of beta-type Ti-40Nb for biomedical use, Surf. Coat. Technol. 302 (2016) 88–99, https://doi.org/10.1016/j.surfcoat.2016.05.036

[6] S. Pilz, A. Gebert, A. Voss, S. Oswald, M. Göttlicher, U. Hempel, J. Eckert, M. Rohnke, J. Janek, M. Calin, Metal release and cell biological compatibility of beta-type Ti-40Nb containing indium, J. Biomed. Mater. Res. - Part B Appl. Biomater. 106 (2018), https://doi.org/10.1002/jbm.b.33976

[7] M. Niinomi, Y. Liu, M. Nakai, H. Liu, H. Li, Biomedical titanium alloys with Young's moduli close to that of cortical bone, Regen. Biomater. 3 (2016) 173–185, https://doi.org/10.1093/RB/RBW016

[8] A. Reck, S. Pilz, M. Kuczyk, A. Gebert, M. Zimmermann, Cyclic deformation characteristics of the metastable β-type Ti–40Nb alloy, Mater. Sci. Eng. A 761 (2019), https://doi.org/10.1016/j.msea.2019.05.096

[9] N. Yumak, K. Aslantas, A review on heat treatment efficiency in metastable b titanium alloys: the role of treatment process and parameters, J. Mater. Res. Technol. 9 (2020) 15360–16280, https://doi.org/10.1016/j.jmrt.2020.10.088

[10] M. Nakai, M. Niinomi, T. Oneda, Improvement in fatigue strength of biomedical β-type Ti-Nb-Ta-Zr alloy while maintaining low young's modulus through optimizing ω-phase precipitation, Metall. Mater. Trans. A Phys. Metall. Mater. Sci. 43 (2012) 294–302, https://doi.org/10.1007/s11661-011-0860-3

[11] A. Reck, S. Pilz, U. Thormann, V. Alt, A. Gebert, M. Calin, C. Heiß, M. Zimmermann, Effects of thermomechanical history and environment on the fatigue behavior of (β)-Ti-Nb implant alloys, MATEC Web Conf. (2018), https://doi.org/10.1051/matecconf/201816506001

[12] H. Matsumoto, S. Watanabe, S. Hanada, Microstructures and mechanical properties of metastable β TiNbSn alloys cold rolled and heat treated, J. Alloy. Compd. 439 (2007) 146–155, https://doi.org/10.1016/j.jallcom.2006.08.267

[13] Y.L. Hao, M. Niinomi, D. Kuroda, K. Fukunaga, Y.L. Zhou, R. Yang, A. Suzuki, Young's modulus and mechanical properties of Ti-29Nb-13Ta-4.6Zr in relation to α″ martensite, Metall. Mater. Trans. A Phys. Metall. Mater. Sci. 33 (2002) 3137–3144, https://doi.org/10.1007/s11661-002-0299-7

[14] T. Akahori, M. Niinomi, H. Fukui, M. Ogawa, H. Toda, Improvement in fatigue characteristics of newly developed beta type titanium alloy for biomedical applications by thermo-mechanical treatments, Mater. Sci. Eng. C 25 (2005) 248–254, https://doi.org/10.1016/j.msec.2004.12.007

[15] T. Akahori, M. Niinomi, H. Fukui, A. Suzuki, Fatigue, fretting fatigue and corrosion characteristics of biocompatible beta type titanium alloy conducted with various thermo-mechanical treatments, Mater. Trans. 45 (2004) 1540–1548, https://doi.org/10.2320/matertrans.45.1540

[16] M. Niinomi, Low modulus titanium alloys for inhibiting bone atrophy, Biomater. Sci. Eng. (2011), https://doi.org/10.5772/24549

[17] X. Zhao, M. Niinomi, M. Nakai, J. Hieda, Beta type Ti-Mo alloys with changeable Young's modulus for spinal fixation applications, Acta Biomater. 8 (2012) 1990–1997, https://doi.org/10.1016/j.actbio.2012.02.004

[18] B. Völker, V. Maier-Kiener, K. Werbach, T. Müller, S. Pilz, M. Calin, J. Eckert, A. Hohenwarter, Influence of annealing on microstructure and mechanical properties of ultrafine-grained Ti45Nb, Mater. Des. 179 (2019) 107864, https://doi.org/10.1016/j.matdes.2019.107864

[19] K. Cho, M. Niinomi, M. Nakai, J. Hieda, R. Kanekiyo, Improvement of tensile and fatigue properties of β-titanium alloy while maintaining low young's modulus through grain refinement and oxygen addition, Mater. Trans. 54 (2013) 2000–2006, https://doi.org/10.2320/matertrans.M2013151

[20] J. Coakley, K.M. Rahman, V.A. Vorontsov, M. Ohnuma, D. Dye, Effect of precipitation on mechanical properties in the β-Ti alloy Ti-24Nb-4Zr-8Sn, Mater. Sci. Eng. A 655 (2016) 399–407, https://doi.org/10.1016/j.msea.2015.12.024

[21] Y.L. Hao, Z.B. Zhang, S.J. Li, R. Yang, Microstructure and mechanical behavior of a Ti-24Nb-4Zr-8Sn alloy processed by warm swaging and warm rolling, Acta Mater. 60 (2012) 2169–2177, https://doi.org/10.1016/j.actamat.2012.01.003

[22] M.J. Lai, T. Li, F.K. Yan, J.S. Li, D. Raabe, Revisiting ω phase embrittlement in metastable β titanium alloys: role of elemental partitioning, Scr. Mater. 193 (2021) 38–42, https://doi.org/10.1016/j.scriptamat.2020.10.031

[23] M. Tane, Y. Okuda, Y. Todaka, H. Ogi, A. Nagakubo, Elastic properties of single-crystalline ω phase in titanium, Acta Mater. 61 (2013) 7543–7554, https://doi.org/10.1016/j.actamat.2013.08.036

[24] S. Banerjee, R. Tewari, G.K. Dey, Omega phase transformation - Morphologies and mechanisms, Int. J. Mater. Res 97 (2006) 963–977, https://doi.org/10.3139/146.101327

[25] A. Gupta, R. Khatirkar, J. Singh, A review of microstructure and texture evolution during plastic deformation and heat treatment of β-Ti alloys, J. Alloy. Compd. 899 (2022) 163242, https://doi.org/10.1016/j.jallcom.2021.163242

[26] S. Hanada, O. Izumi, Transmission electron microscopic observations of mechanical twinning in metastable beta titanium alloys, Metall. Trans. A. 17 (1986) 1409–1420, https://doi.org/10.1007/BF02650122

[27] S. Hanada, T. Yoshio, O. Izumi, Effect of plastic deformation modes on tensile properties of beta titanium alloys, Trans. Jpn. Inst. Metals 27 (1986) 496–503 ⟨https://doi.org/10.2320/matertrans1960.27.496⟩.

[28] M. Oka, Y. Taniguchi, {332} Deformation twins in a Ti-15.5 pct V alloy, Metall. Trans. A 10 (1979) 651–653, https://doi.org/10.1007/BF02658330

[29] L. Ren, W. Xiao, D. Kent, M. Wan, C. Ma, L. Zhou, Simultaneously enhanced strength and ductility in a metastable β-Ti alloy by stress-induced hierarchical twin structure, Scr. Mater. 184 (2020) 6–11, https://doi.org/10.1016/j.scriptamat.2020.03.039

[30] K. Cho, R. Morioka, S. Harjo, T. Kawasaki, H.Y. Yasuda, Study on formation mechanism of {332} < 113 > deformation twinning in metastable β-type Ti alloy focusing on stress-induced α" martensite phase, Scr. Mater. 177 (2020) 106–111, https://doi.org/10.1016/j.scriptamat.2019.10.011

[31] J. Zhang, B. Qian, W. Lin, P. Zhang, Y. Wu, Y. Fu, Y. Fan, Z. Chen, J. Cheng, J. Li, Y. Wu, Y. Wang, F. Sun, Compressive deformation-induced hierarchical microstructure in a TWIP β Ti-alloy, J. Mater. Sci. Technol. 112 (2022) 130–137, https://doi.org/10.1016/j.jmst.2021.09.048

[32] X. Zhao, M. Niinomi, M. Nakai, J. Hieda, T. Ishimoto, T. Nakano, Optimization of Cr content of metastable β-type Ti-Cr alloys with changeable Youngs modulus for spinal fixation applications, Acta Biomater. 8 (2012) 2392–2400, https://doi.org/10.1016/j.actbio.2012.02.010

[33] H.Y. Kim, S. Miyazaki, Martensitic transformation and superelastic properties of Ti-Nb base alloys, Mater. Trans. 56 (2015) 625–634, https://doi.org/10.2320/matertrans.M2014454

[34] S.A. Mantri, F. Sun, D. Choudhuri, T. Alam, B. Gwalani, F. Prima, R. Banerjee, Deformation induced hierarchical twinning coupled with omega transformation in a metastable β-Ti alloy, Sci. Rep. 9 (2019) 1334, https://doi.org/10.1038/s41598-018-37865-0

[35] M.J. Lai, C.C. Tasan, J. Zhang, B. Grabowski, L.F. Huang, D. Raabe, Origin of shear induced β to ω transition in Ti-Nb-based alloys, Acta Mater. 92 (2015) 55–63, https://doi.org/10.1016/j.actamat.2015.03.040

[36] K. Chen, Q. Fan, J. Yao, L. Yang, S. Xu, Y. Gao, W. Lei, Influence of stress-induced α" phase transformation on mechanical properties in metastable β type Ti-5Al-2.5Cr-5Mo-1Sn alloy, J. Alloy. Compd. 920 (2022) 165563, https://doi.org/10.1016/j.jallcom.2022.165563

[37] M.J. Lai, T. Li, D. Raabe, Ω phase acts as a switch between dislocation channeling and joint twinning- and transformation-induced plasticity in a metastable β titanium alloy, Acta Mater. 151 (2018) 67–77, https://doi.org/10.1016/j.actamat.2018.03.053

[38] S.A. Mantri, D. Choudhuri, T. Alam, V. Ageh, F. Sun, F. Prima, R. Banerjee, Change in the deformation mode resulting from beta-omega compositional partitioning in a Ti[sbnd]Mo alloy: room versus elevated temperature, Scr. Mater. 130 (2017) 69–73, https://doi.org/10.1016/j.scriptamat.2016.11.013

[39] S. Hanada, M. Ozeki, O. Izumi, Deformation characteristics in B phase Ti-Nb alloys, Metall. Trans. A 16 (1985) 789–795, https://doi.org/10.1007/BF02814829

[40] J. Gao, A.J. Knowles, D. Guan, W.M. Rainforth, ω phase strengthened 1.2GPa metastable β titanium alloy with high ductility, Scr. Mater. 162 (2019) 77–81, https://doi.org/10.1016/j.scriptamat.2018.10.043

[41] J.F. Xiao, Z.H. Nie, Z.W. Ma, G.F. Liu, F. Hao, C.W. Tan, ω precipitation: deformation regulator in metastable titanium alloys, Mater. Sci. Eng. A 772 (2020) 138687, https://doi.org/10.1016/j.msea.2019.138687

[42] W. Chen, S. Cao, W. Kou, J. Zhang, Y. Wang, Y. Zha, Y. Pan, Q. Hu, Q. Sun, J. Sun, Origin of the ductile-to-brittle transition of metastable β-titanium alloys: self-hardening of ω-precipitates, Acta Mater. 170 (2019) 187–204, https://doi.org/10.1016/j.actamat.2019.03.034

[43] W. Wang, X. Zhang, W. Mei, J. Sun, Role of omega phase evolution in plastic deformation of twinning-induced plasticity β Ti–12V–2Fe–1Al alloy, Mater. Des. 186 (2020), https://doi.org/10.1016/j.matdes.2019.108282

[44] H.Y. Kim, Y. Ikehara, J.I. Kim, H. Hosoda, S. Miyazaki, Martensitic transformation, shape memory effect and superelasticity of Ti-Nb binary alloys, Acta Mater. 54 (2006) 2419–2429, https://doi.org/10.1016/j.actamat.2006.01.019

[45] M. Tahara, H.Y. Kim, T. Inamura, H. Hosoda, S. Miyazaki, Lattice modulation and superelasticity in oxygen-added β-Ti alloys, Acta Mater. 59 (2011) 6208–6218, https://doi.org/10.1016/j.actamat.2011.06.015

[46] H. Liu, M. Niinomi, M. Nakai, X. Cong, K. Cho, C.J. Boehlert, V. Khademi, Abnormal deformation behavior of oxygen-modified β-type Ti-29Nb-13Ta-4.6Zr alloys for biomedical applications, Metall. Mater. Trans. A Phys. Metall. Mater. Sci. 48 (2017) 139–149, https://doi.org/10.1007/s11661-016-3836-5

[47] L.S. Wei, H.Y. Kim, S. Miyazaki, Effects of oxygen concentration and phase stability on nano-domain structure and thermal expansion behavior of Ti-Nb-Zr-Ta-O alloys, Acta Mater. 100 (2015) 313–322, https://doi.org/10.1016/j.actamat.2015.08.054

[48] M.J. Lai, C.C. Tasan, D. Raabe, Deformation mechanism of ω-enriched Ti-Nb-based gum metal: dislocation channeling and deformation induced ω-β

transformation, Acta Mater. 100 (2015) 290–300, https://doi.org/10.1016/j.actamat.2015.08.047
[49] D. Choudhuri, S.A. Mantri, T. Alam, S. Banerjee, R. Banerjee, Precipitate-dislocation interaction mediated Portevin-Le Chatelier-like effect in a beta-stabilized Ti-Mo-Nb-Al alloy, Scr. Mater. 124 (2016) 15–20, https://doi.org/10.1016/j.scriptamat.2016.06.043
[50] S. Banerjee, U.M. Naik, Plastic instability in an omega forming Ti-15% Mo alloy, Acta Mater. 44 (1996) 3667–3677, https://doi.org/10.1016/1359-6454(96)00012-2
[51] S. Pilz, D. Geissler, M. Calin, J. Eckert, M. Zimmermann, J. Freudenberger, A. Gebert, Thermomechanical processing of In-containing β-type Ti-Nb alloys, J. Mech. Behav. Biomed. Mater. 79 (2018), https://doi.org/10.1016/j.jmbbm.2017.12.028
[52] M. Bönisch, A. Panigrahi, M. Calin, T. Waitz, M. Zehetbauer, W. Skrotzki, J. Eckert, Thermal stability and latent heat of Nb–rich martensitic Ti-Nb alloys, J. Alloy. Compd. 697 (2017) 300–309, https://doi.org/10.1016/j.jallcom.2016.12.108
[53] D.L. Moffat, D.C. Larbalestier, The competition between the alpha and omega phases in aged Ti-Nb alloys, Metall. Trans. A 19 (1988) 1687–1694, https://doi.org/10.1007/BF02645136
[54] M. Calin, A. Helth, J.J. Gutierrez Moreno, M. Bönisch, V. Brackmann, L. Giebeler, T. Gemming, C.E. Lekka, A. Gebert, R. Schnettler, J. Eckert, Elastic softening of β-type Ti-Nb alloys by indium (In) additions, J. Mech. Behav. Biomed. Mater. 39 (2014) 162–174, https://doi.org/10.1016/j.jmbbm.2014.07.010
[55] F. Bachmann, R. Hielscher, H. Schaeben, Texture analysis with MTEX- Free and open source software toolbox, Solid State Phenom. 160 (2010) 63–68, https://doi.org/10.4028/www.scientific.net/SSP.160.63
[56] N. Schell, A. King, F. Beckmann, T. Fischer, M. Müller, A. Schreyer, The high energy materials science beamline (HEMS) at PETRA III, Mater. Sci. Forum 772 (2013) 57–61, https://doi.org/10.4028/www.scientific.net/MSF.772.57
[57] L. Lutterotti, D. Chateigner, S. Ferrari, J. Ricote, Texture, residual stress and structural analysis of thin films using a combined X-ray analysis, Thin Solid Films 450 (2004) 34–41, https://doi.org/10.1016/j.tsf.2003.10.150
[58] M. Hansen, E.L. Kamen, H.D. Kessler, D.J. McPherson, Systems titanium-molybdenum and titanium-columbium, JOM 3 (1951) 881–888, https://doi.org/10.1007/BF03397396
[59] J.M. Silcock, M.H. Davies, H.K. Hardy, Structure of the ω-precipitate in titanium–16 per cent vanadium alloy, Nature 175 (1955) 731-731, https://doi.org/10.1038/175731a0
[60] A.R.G. Brown, D. Clark, J. Eastabrook, K.S. Jepson, The titanium–niobium system, Nature 201 (1964) 914–915, https://doi.org/10.1038/201914a0
[61] M. Abdel-Hady, K. Hinoshita, H. Fuwa, Y. Murata, M. Morinaga, Change in anisotropy of mechanical properties with β-phase stability in high Zr-containing Ti-based alloys, Mater. Sci. Eng. A 480 (2008) 167–174, https://doi.org/10.1016/j.msea.2007.06.083
[62] T. Inamura, R. Shimizu, H.Y. Kim, S. Miyazaki, H. Hosoda, Optimum rolling ratio for obtaining {001} < 110 > recrystallization texture in Ti-Nb-Al biomedical shape memory alloy, Mater. Sci. Eng. C 61 (2016) 499–505, https://doi.org/10.1016/j.msec.2015.12.086
[63] M. Tahara, H.Y. Kim, H. Hosoda, S. Miyazaki, Cyclic deformation behavior of a Ti-26 at% Nb alloy, Acta Mater. 57 (2009) 2461–2469, https://doi.org/10.1016/j.actamat.2009.01.037
[64] S. Guo, Y. Shang, J. Zhang, Q. Meng, X. Cheng, X. Zhao, In situ synchrotron X-ray diffraction study of stress-induced martensitic transformation in a metastable β-type Ti-33Nb-4Sn alloy, Intermetallics 86 (2017) 20–24, https://doi.org/10.1016/j.intermet.2017.03.009
[65] S. Guo, Y. Shang, J. Zhang, Q. Meng, X. Cheng, X. Zhao, In situ synchrotron X-ray diffraction study of deformation behaviour of a metastable β-type Ti-33Nb-4Sn alloy, Mater. Sci. Eng. A 692 (2017) 81–89, https://doi.org/10.1016/j.msea.2017.03.061
[66] W. Oliferuk, M. Maj, Plastic instability criterion based on energy conversion, Mater. Sci. Eng. A 462 (2007) 363–366, https://doi.org/10.1016/j.msea.2006.02.465
[67] M.J. Lai, C.C. Tasan, D. Raabe, On the mechanism of {332} twinning in metastable β titanium alloys, Acta Mater. 111 (2016) 173–186, https://doi.org/10.1016/j.actamat.2016.03.040
[68] E. Bertrand, P. Castany, T. Gloriant, An alternative way to orient the parent phase in the cubic/orthorhombic martensitic transformation of titanium shape memory alloys, Scr. Mater. 83 (2014) 41–44, https://doi.org/10.1016/j.scriptamat.2014.04.012
[69] M. Abdel-Hady, K. Hinoshita, M. Morinaga, General approach to phase stability and elastic properties of β-type Ti-alloys using electronic parameters, Scr. Mater. 55 (2006) 477–480, https://doi.org/10.1016/j.scriptamat.2006.04.022
[70] S. Hanada, O. Izumi, Correlation of tensile properties, deformation modes, and phase stability in commercial β-phase titanium alloys, Metall. Trans. A 18 (1987) 265–271, https://doi.org/10.1007/BF02825707
[71] H.Y. Kim, H. Satoru, J. Il Kim, H. Hosoda, S. Miyazaki, Mechanical properties and shape memory behavior of Ti-Nb alloys, Mater. Trans. 45 (2004) 2443–2448, https://doi.org/10.2320/matertrans.45.2443
[72] E.L. Pang, E.J. Pickering, S.I. Baik, D.N. Seidman, N.G. Jones, The effect of zirconium on the omega phase in Ti-24Nb-[0–8]Zr (at%) alloys, Acta Mater. 153 (2018) 62–70, https://doi.org/10.1016/j.actamat.2018.04.016
[73] J. Il Kim, H.Y. Kim, H. Hosoda, S. Miyazaki, Shape memory behavior of Ti-22Nb-0.5–2.0 O(at%) biomedical alloys, Mater. Trans. 46 (2005) 852–857, https://doi.org/10.2320/matertrans.46.852
[74] S. Hanada, T. Ozaki, E. Takahashi, S. Watanabe, K. Yoshimi, T. Abumiya, Composition dependence of Young's modulus in beta titanium binary alloys, Mater. Sci. Forum 426–432 (2003) 3103–3108, https://doi.org/10.4028/www.scientific.net/msf.426-432.3103
[75] F. Sun, J.Y. Zhang, P. Vermaut, D. Choudhuri, T. Alam, S.A. Mantri, P. Svec, T. Gloriant, P.J. Jacques, R. Banerjee, F. Prima, Strengthening strategy for a ductile metastable β-titanium alloy using low-temperature aging, Mater. Res. Lett. 5 (2017) 547–553, https://doi.org/10.1080/21663831.2017.1350211
[76] M. Bönisch, M. Calin, L. Giebeler, A. Helth, A. Gebert, W. Skrotzki, J. Eckert, Composition-dependent magnitude of atomic shuffles in Ti-Nb martensites, J. Appl. Crystallogr. 47 (2014) 1374–1379, https://doi.org/10.1107/S1600576714012576
[77] X. Zhou, X. a Min, S. Emura, K. Tsuchiya, Accommodative {332}〈113〉 primary and secondary twinning in a slightly deformed β-type Ti-Mo titanium alloy, Mater. Sci. Eng. A 684 (2017) 456–465, https://doi.org/10.1016/j.msea.2016.12.025